Simultaneous in situ measurements of small-scale structures in neutral, plasma, and atomic oxygen densities during WADIS sounding rocket project

Boris Strelnikov[1], Martin Eberhart[4], Martin Friedrich[5], Jonas Hedin[3], Mikhail Khaplanov[3†],
Gerd Baumgarten[1], Bifford P. Williams[6], Tristan Staszak[1], Heiner Asmus[1], Irina Strelnikova[1],
Ralph Latteck[1], Mykhaylo Grygalashvyly[1], Franz-Josef Lübken[1], Josef Höffner[1], Raimund Wörl[1],
Jörg Gumbel[3], Stefan Löhle[4], Stefanos Fasoulas[4], Markus Rapp[2], Aroh Barjatya[7], Michael J. Taylor[8],
and Pierre-Dominique Pautet[8]

[1]Leibniz-Institute of Atmospheric Physics at the Rostock University, Kühlungsborn, Germany
[2]Deutsches Zentrum für Luft- und Raumfahrt, Institut für Physik der Atmosphäre, Oberpfaffenhofen, Germany
[3]Department of Meteorology (MISU), Stockholm University, Stockholm, Sweden
[4]University of Stuttgart, Institute of Space Systems, Stuttgart, Germany
[5]Graz University of Technology, Graz, Austria
[6]GATS, Boulder, USA
[7]Embry-Riddle Aeronautical University, FL, USA
[8]Center for Atmospheric and Space Sciences, Utah State University, Logan, Utah, USA
[†]Deceased

Correspondence: B. Strelnikov (strelnikov@iap-kborn.de)

Abstract. In this paper we present an overview of measurements conducted during the WADIS-2 rocket campaign. We investigate the effect of small-scale processes like gravity waves and turbulence on the distribution of atomic oxygen and other species in the MLT region. Our analysis suggests that density fluctuations of atomic oxygen are coupled to fluctuations of other constituents, i.e., plasma and neutrals. Our measurements show that all measured quantities, including winds, densities, and temperatures, reveal signatures of both waves and turbulence. We show observations of gravity wave saturation and breakdown together with simultaneous measurements of generated turbulence. Atomic oxygen inside turbulence layers shows two different spectral behaviors, which might imply change of its diffusion properties.

1 Introduction

The mesosphere, lower thermosphere (MLT) region is host of phenomena that are connected to dynamic and chemical processes which are still not fully understood. Thus, e.g., it is generally accepted that atmospheric gravity waves (GW) play an essential role in the dynamics of this region and that they couple it with the lower and upper atmosphere (e.g., Becker and Schmitz, 2002; Fritts and Alexander, 2003; Alexander et al., 2010). When propagating, GW might dissipate and thereby generate turbulence. Apart of the momentum deposition, which is a key coupling process, this also affects mixing and redistribution of trace constituents. One of the most important trace constituents in MLT is atomic oxygen (O) which plays an essential role in the chemistry and energy budget of the mesopause region (e.g., Mlynczak and Solomon, 1993). It is the major reactive

trace constituent in the mesosphere/lower thermosphere (MLT) region and it plays a crucial role in different chemical reactions involved in airglow excitation or ion chemistry (e.g., Walterscheid et al., 1987; McDade et al., 1986; McDade, 1998; Marsh et al., 2006; Caridade et al., 2013; Lednyts'kyy et al., 2015). The lifetime of atomic oxygen varies with altitude from seconds at ∼50 km to months at ∼100 km (e.g., Torr, 1985; Smith et al., 2010).

5   Chemical heat released during exothermic reactions involving atomic oxygen is one of the main contributors to the energy budget of this region (e.g., Mlynczak and Solomon, 1991; Mlynczak and Solomon, 1993). These reactions yield chemical heating rates in the mesopause region of several K/day which is comparable (or even competitive) to those of turbulent heating as well as direct heating due to solar radiation. Oxygen is involved in exothermic reactions with hydroxyl (OH) which emission bands have been extensively used to study the mesopause-region temperature, gravity waves, and tides (e.g., Hines and Tarasick,
10 1987; Taylor et al., 1995, 1997, 2009; Snively, 2013; Fritts et al., 2014; Egito et al., 2017, and references therein).

    It is believed that at altitudes where the O-lifetime is very long, i.e., roughly above 90 km, variations in O-density manly result from dynamical processes such as GW, tides, and the large scale circulation. Whereas at lower heights chemical processes may play a crucial role in forming O-density variations. It is also known, that mesopause region is very active dynamically. It is region where GW break and a persistent turbulence field plays crucial role in global circulation (e.g., Becker and Schmitz,
15 2002; Fritts and Alexander, 2003; Rapp et al., 2004). However, it is not known, for instance, how turbulence influences the O-density distribution, its diffusion properties and whether it can affects chemical heat release e.g., by changing reaction rates.

    This implies that in order to properly characterize the chemical and dynamical state of the mesopause region, it is important to know the altitude resolved concentration of atomic oxygen alongside with the state of the background atmosphere including its thermal structure and dynamical parameters.

20   All these aspects stress the importance of common-volume measurements of the oxygen density together with temperature and density of the background neutral atmosphere with a sufficiently high altitude resolution.

    This paper aims at two things. First, it is to provide an overview of the WADIS-2 sounding rocket campaign and measured parameters, and second, to study the effect of gravity wave motions and turbulence on the distribution of atomic oxygen in the nighttime MLT region. We present results of in situ and some ground based measurements obtained in the frame of the WADIS
25 sounding rocket mission. We introduce new high resolution O-density measurements in connection with other parameters of the atmosphere. The paper is structured as follows. In Sec. 2 we briefly describe the WADIS-2 mission and measurement techniques used in this study. In Sec. 3 we present measurement results followed by a more detailed analysis in Sec. 4. In Sec. 5 we critically discuss the our findings and finally, in Sec. 6 we summarize main results and give an outlook to our next rocket borne measurements.

30 2   WADIS-2 rocket campaign and instrumentation

The WADIS sounding rocket mission led by the Leibniz-Institute of Atmospheric Physics (IAP) in Kühlungsborn, Germany, in partnership with the Institute of Space Systems (IRS) in Stuttgart and contributions from Austria, Sweden, the USA, and Norway, comprised two field campaigns conducted at the Andøya Space Center (ACS) in northern Norway (69°N, 16°E).
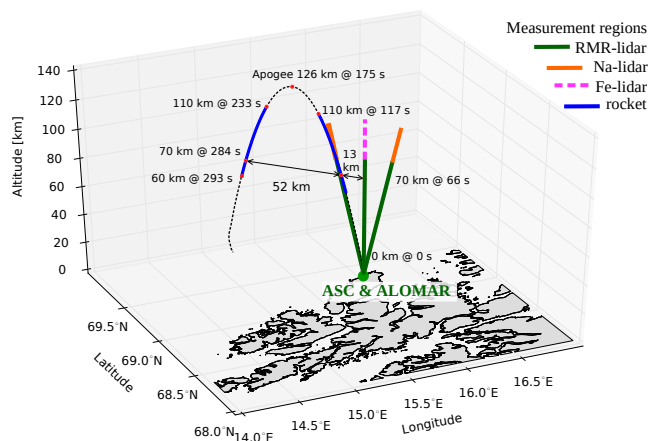
Figure 1. Schematics of WADIS-2 rocket experiment. Solid green and orange, and dashed magenta lines show ALOMAR RMR-, Na-, and IAP Fe-lidar measurement volumes, respectively. Black dashed line shows rocket trajectory. Blue lines show rocket measurement range used in this study.

The first campaign was conducted in June 2013 and the second in March 2015. WADIS stands for "Wave propagation and dissipation in the middle atmosphere: Energy budget and distribution of trace constituents". The mission aimed at studying the propagation and dissipation of gravity waves (GW) and measuring concentration of atomic oxygen simultaneously. Such measurements allow for estimation of the contribution of chemical and turbulent heating to the energy budget of the MLT, as well as the transport of atomic oxygen by waves and turbulence. For a more detailed mission description the reader is referred to Strelnikov et al. (2017). The Arctic Lidar Observatory for Middle Atmosphere Research (ALOMAR, von Zahn et al., 1995) is located close the launch site and was an integral part of the entire WADIS mission.

The launch window for the second sounding rocket campaign was scheduled around local midnight to ensure full nighttime conditions. A large number of ground-based optical instruments were supporting the WADIS-2 rocket campaign. The ALOMAR RMR-, Na Weber, and IAP Fe-lidar were running continuously throughout the campaign period whenever weather permitted. Also the Advanced Mesospheric Temperature Mapper (AMTM) by Utah State University (Pautet et al., 2014) was observing the night glow emissions at 1523.68 and 1542.79 nm.

The Middle Atmosphere ALOMAR Radar System, MAARSY, (Rapp et al., 2011; Latteck et al., 2012) operated by IAP located close to the rocket launch site was continuously running. MAARSY was used to detect polar mesospheric winter echoes (PMWE) in case they should occur (Latteck and Strelnikova, 2015).

The instrumented WADIS-2 payload was almost identical to that one launched during the first campaign (see Strelnikov et al., 2017, for details), except that the instruments were tuned for the polar night launch conditions.

The front and rear decks of the WADIS payloads were equipped with identical CONE ionization gauges to measure turbulence, neutral air density, and temperature on up- and downleg (Strelnikov et al., 2013). A positive ion probe (PIP) operated by the University of Technology in Graz (TUG), Austria, and novel Langmuir probe (LP) developed and operated by Embry-

Riddle Aeronautical University in Florida, USA, yielded high-resolution positive ion and electron density measurement, respectively. Both these plasma probes were mounted on booms located on the rear deck of the payload.

Two instruments, the FIPEX and an airglow photometer, were used to measure atomic oxygen densities. These instruments, utilized entirely different measurement techniques. Photometers yield precise absolute density measurements, whereas FIPEX yields high altitude resolution data. The absolute values of the FIPEX-measurements were validated by the Photometers (see Eberhart et al., 2018, for more details).

The FIPEX instruments developed by IRS, yield profiles of atomic oxygen densities with high altitude resolution of ~20 m (see Eberhart et al., 2015). Photometers operated by the Meteorological Institute at Stockholm University (MISU) measured oxygen densities using a well established reliable technique applied before on a large number of sounding rockets (e.g., Hedin et al., 2009).

The WADIS-2 sounding rocket was launched on 5th of March 2015 at 01:44:00 UTC, that is during full night-time conditions. Fig. 1 shows the geometry of the WADIS-2 experiment. The black dashed parabola shows the actual rocket trajectory. The blue profiles show parts of the rocket trajectory which yielded measurements used in this paper. The solid green, orange, and dashed magenta lines show direction and altitude range for RMR-, Na, and Fe-lidar, respectively. It is seen, that the north-west (NW) directed lidar beam was co-located with the ascending part of the rocket trajectory.

3 Data

In this section we show data obtained by ground-based instruments around the rocket launch time and some profiles measured on board the WADIS-2 sounding rocket. We start with measurements of the background state of the atmosphere as observed during the night of the rocket launch. Then we compare upleg and downleg density measurements conducted by different instruments. These profiles are then used in Sec. 4 for a detailed fluctuation analysis. Finally, we demonstrate that the high-resolution FIPEX-measurements yielded new, geophysically meaningful data.

3.1 Background

The background state of the atmosphere was continuously monitored by the ALOMAR lidars and radars. MAARSY did not observe any echoes during the night of the rocket launch. That is, the WADIS-2 rocket launch was under conditions of confirmed absence of polar mesospheric winter echoes, PMWE. Thanks to favorable weather conditions, the lidars were able to measure both temperature and wind fields for several hours around rocket launch time.

Fig. 2 shows the temperature field measured by the IAP RMR- and Fe-lidars from 20 up to ~100 km altitude around the time of the WADIS-2 rocket launch. Signatures of long period waves are clearly seen above ~65 km altitude. Horizontal temperature field observed by the AMTM (Pautet et al., 2014) shown in Fig. 3 also reveals clear large scale structures around the WADIS-2 launch time. Wörl et al. (2018) analyzed the co-located temperature measurements by both Fe-lidar and AMTM in detail and concluded that the most pronounced wave signatures reveal periods of 24, 12, and 8 hours i.e., they are most probably created by tides.
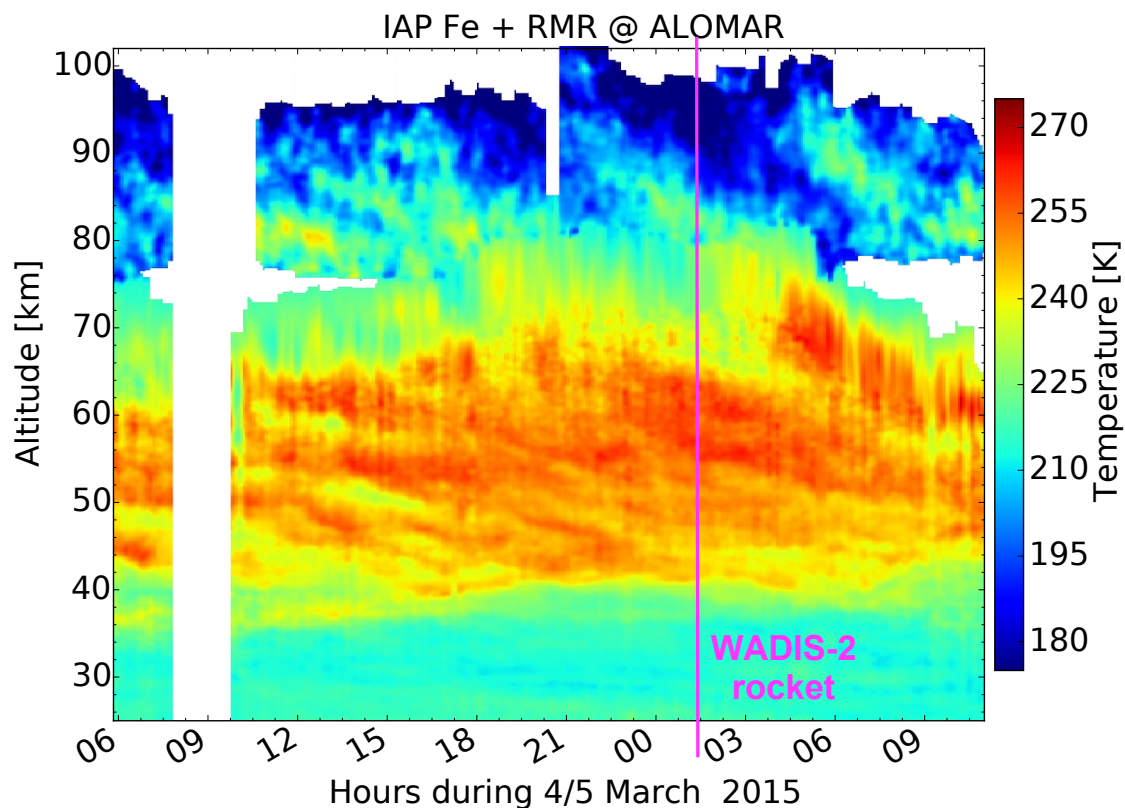
Figure 2. Combined RMR- and Fe-lidar temperature measurements during the night of the WADIS-2 rocket launch, i.e. 4 to 5 of March 2015.
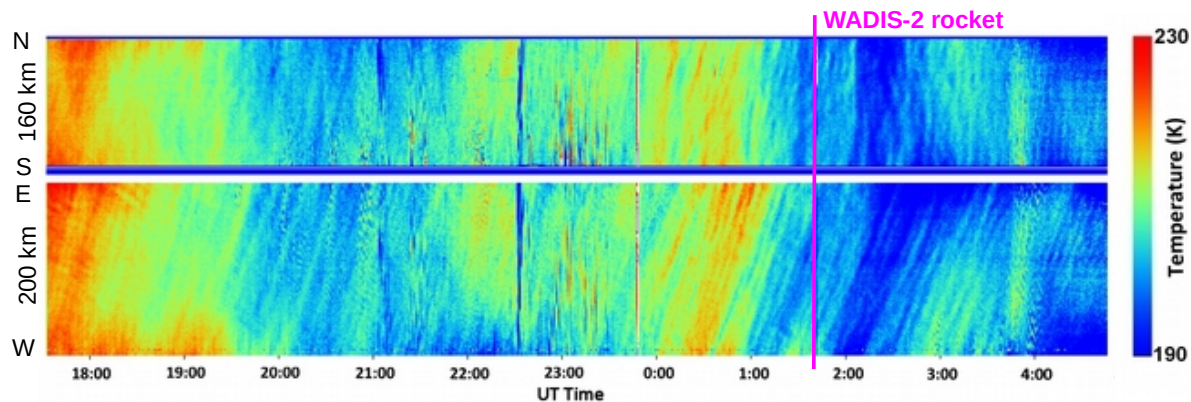
Figure 3. NS and WE keogram summary of the AMTM temperature measurements obtained during the night of 4 to 5 March 2015.

(a) North-West beam, i.e. close to rocket trajectory.

(b) South-East beam.
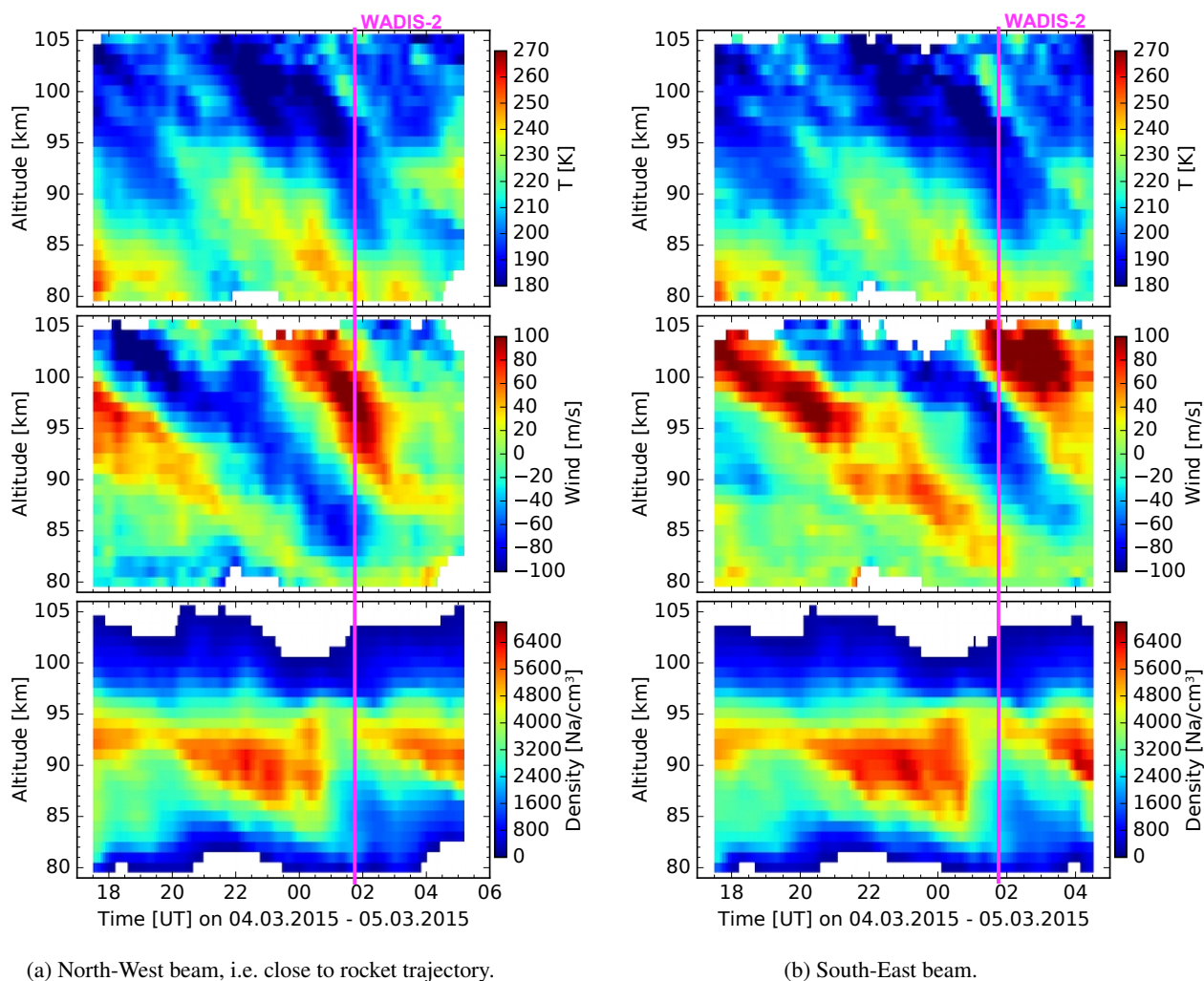
Figure 4. Na-lidar measurements during the night of the WADIS-2 rocket launch, i.e. 4 to 5 of March 2015. Rocket was launched at 1:44 UT

Fig. 4 shows measurements by the Na-lidar conducted throughout the night of the WADIS-2 launch. Similar to Fe-temperature these measurements show prominent signatures of long period waves above 80 km altitude in both temperature and wind fields.

All these data contain also smaller scale fluctuations which result from gravity waves and turbulence. To see such small-scale fluctuations better and analyze them properly, one has to subtract the large-scale background (including tides) from the
5   measurements shown in Fig. 2, 3, and 4 (see e.g., Strelnikova et al., 2018). In the next section we focus on small-scale fluctuations of different quantities. We analyze rocket-borne instant measurements and further compare these with profiles measured by the ground-based instruments at the time of rocket launch.

3.2 In-situ measurements

The WADIS-2 rocket was launched at 1:44 UTC and reached an apogee of 126 km. The measurement phase started at about
10   60 km altitude after nose-cone and motor separation. However the best quality data was obtained above 70 km height, mostly due to favorable aerodynamic conditions.
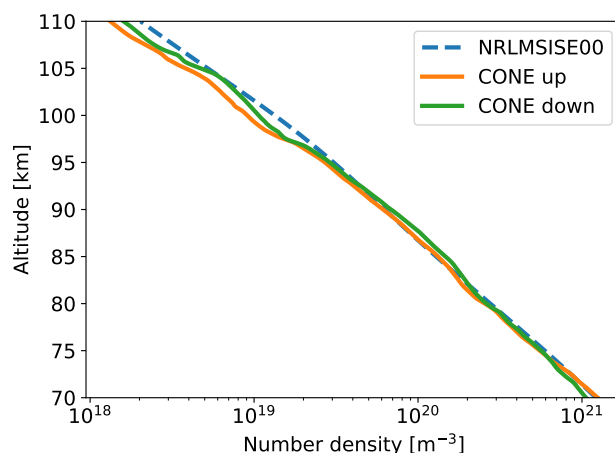
Figure 5. Rocket-borne density measurements by the ionization gauge CONE for upleg and downleg (orange and green lines, respectively). Blue dashed line shows the NRL-MSISE00 climatology for the time of WADIS-2 launch, i.e. 5 of March 2015, 01:44:00 UTC.

Figs. 5 and 6 show in situ measured profiles of neutral air densities and temperatures. Orange and green lines show up- and downleg measurements, respectively. Blue dashed profiles represent NRLMSISE-00 reference atmosphere (Picone et al., 2002). Both up- and downleg profiles look very similar in terms of mean values and oscillations. The background atmosphere
15   reveals a typical winter state (see e.g., Strelnikov et al., 2013, where a collection of rocket-borne measurements for different seasons is shown). Also, the observed turbulence activity shown in Sec. 4 demonstrates a typical for winter behavior. The temperature profiles clearly show some GW-signatures at altitudes below 80 km. The height range between ∼83 and 90 km reveals very low GW amplitudes. A temperature increase of ∼40 K reminiscent of mesospheric inversion layers (MIL) similar to those analyzed by Szewczyk et al. (2013) is seen between 95 and 100 km and is discussed in Sec. 4.
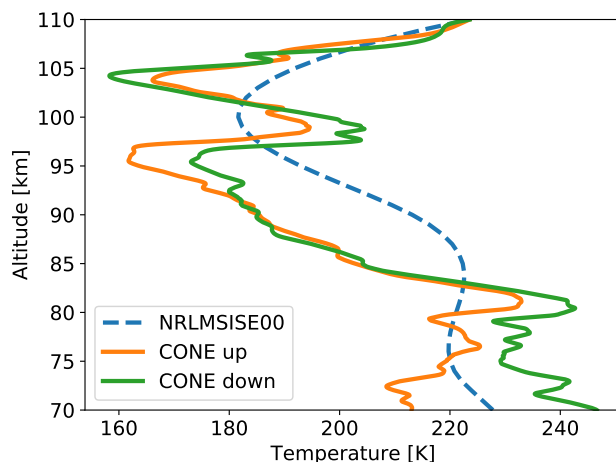
Figure 6. Temperatures derived from the densities shown in Fig. 5 assuming hydrostatic equilibrium.
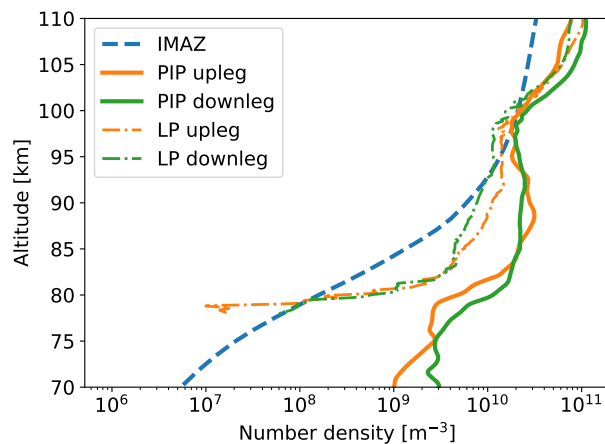
Figure 7. Same as Fig. 5 but for positive ion (solid lines) and electron (dash-dotted profiles) densities measured by the PIP and LP instruments, respectively. Blue dashed line shows empirical ionospheric model for the auroral zone, IMAZ, derived for the time of the WADIS-2 flight.

The neutral density profiles in Fig. 5 also show some oscillations that can be attributed to gravity waves, which will be analyzed in detail in Sec. 4.

In Fig. 7 we show profiles of electron and positive ion densities measured in-situ on both up- and downleg. Dashed-dotted and solid profiles show electron and positive ion data, respectively. The two ion density profiles are also quite similar and also reveal some wave signatures. The two electron density profiles also demonstrate that ionospheric background at the rocket up- and downleg is rather similar. Comparison with an empirical ionospheric model for the auroral zone, IMAZ (McKinnell and Friedrich, 2007) shown in Fig. 7 (blue dashed line) shows that ionization level of the ionosphere was moderately high. This
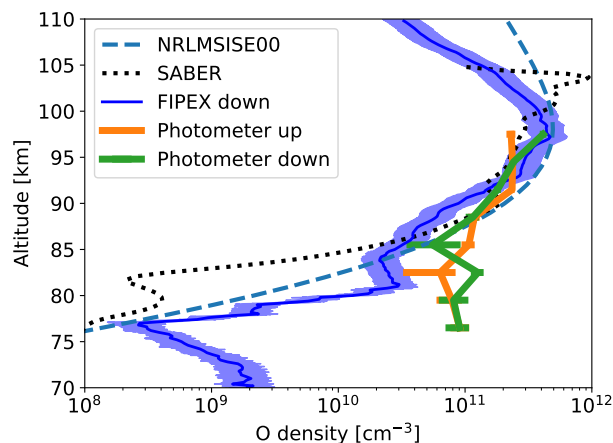
Figure 8. Same as Fig. 5 but for atomic oxygen densities measured by photometers. Additionally, FIPEX downleg data is shown by blue profile with shaded area showing measurement errors and black dotted line shows SABER measurements (Level 2A, O event 20 orbit 71729).

is in accord with the fact that some aurora was seen throughout the night of these observations. Also, the auroral emission detector operated together with the airglow photometer by MISU registered some auroral emissions above 100 km height. The shown plasma density profiles yield relative density measurements and therefore, they were normalized to wave propagation experiment values at altitudes of ∼115 km (see e.g., Friedrich, 2016; Asmus et al., 2017, for more details). The large difference between positive ion and electron densities at altitudes ∼80–95 km was studied in detail by Asmus et al. (2017) and was shown to be due to charged dust particles.

Fig. 8 shows atomic oxygen density profiles measured by the photometer on up- and downleg in orange and green, respectively. The FIPEX measurements are only shown for the descending part of the WADIS-2 rocket flight, because we are mostly confident in their absolute values and will use this data for further analysis. The blue dashed line shows NRLMSIS-00 data and black dotted line shows SABER retrievals (orbit 71729, event 20) at ∼230 km distant location and ∼4 h before rocket launch. That is, the SABER measurements were not collocated and not simultaneous with the rocket flight and are only shown for qualitative comparison. However, the apparent density increase in SABER data above 100 km must rather be attributed to the observed auroral activity.

It is already seen in Fig. 8 that the O-density profiles reveal some oscillations with largest amplitudes below approx. 83 km altitude. It is worth mentioning, that other FIPEX sensors yielded fluctuations data that show the same features (not shown here and discussed in detail in Eberhart et al., 2018)

The photometer measurements have an effective altitude resolution of 3 km, whereas the catalytic FIPEX sensors exhibit height resolution of ∼20 m. In the next section we examine which advantages the high resolution measurements of the atomic oxygen densities can bring and what the nature of the fluctuations in the FIPEX data is.
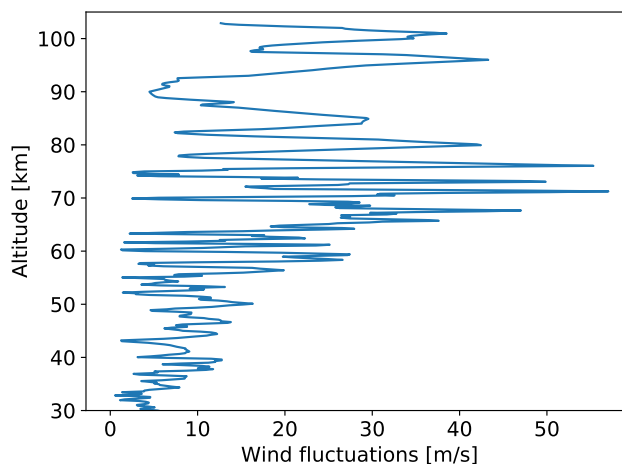
Figure 9. Horizontal wind fluctuations (i.e., $\sqrt{u'^2 + v'^2}$, where u' and v' are zonal and meridional wind fluctuations) derived from combined RMR- and Na-lidar measurements for the time of WADIS-2 rocket flight.

4   Analysis

To extract small-scale fluctuations from the measured profiles, we subtract the mean background derived as running average over 5 km long vertical window. Similar results can be achieved by e.g., applying a polynomial fit of the same vertical resolution, i.e. 5 km or by means of other techniques (e.g., Strelnikova et al., 2018). We here focus on small vertical length scales

5   <5 km comprising both turbulent fluctuations as well as part of the gravity wave spectrum. We note that choosing a particular cut off wavelength always carries some degree of arbitrariness. For the small-scale stuff and, especially turbulent structures, the background derivation does not affect the data analysis if residual fluctuations data contain all the scales below this limit (i.e. ~5 km).

Fluctuations of horizontal wind derived from the lidar measurements for the time of the WADIS-2 rocket launch are shown in

10   Fig. 9. It reveals an amplitude increase with height, z, according to the exponential law ($\propto \exp(z/2H)$, where H is scale height). It demonstrates basically, that we observed gravity waves in the entire altitude range from near the ground up to ~105 km. Wind fluctuation amplitude increases in the altitude range from 30 up to ~70 km. Then the amplitude drops within altitude range 70 to 80 km and increases again between 88 and 95 km. This is consistent with the behavior of temperature profiles that show larger wave amplitudes below 80 km altitude, very low amplitudes above that height and large wave amplitude again

15   between 95 and 105 km (Figs. 4 and 6).

In Fig. 10 we show relative density fluctuations (residuals) for neutrals, positive ions, and atomic oxygen in blue, orange, and green, respectively. All three profiles show wave-like oscillations with (vertical) wavelengths in the range 1 to 5 km that can be attributed to gravity waves. Between 103 and 110 km altitude all three profiles oscillate in phase. Below ~103 km height these density fluctuations reveal similar wavelengths but shifted in phase relative to each other.
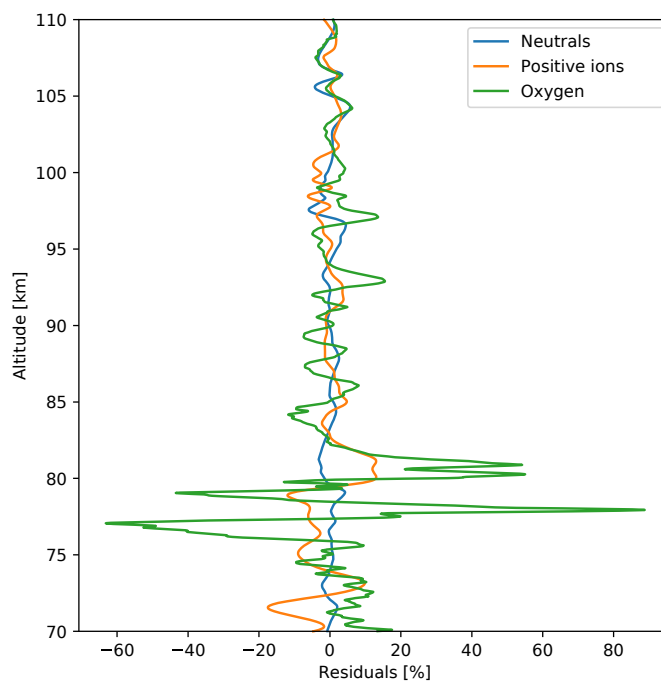
Figure 10. Relative density fluctuations (=residuals) of neutral air, positive ions, and atomic oxygen shown by blue, orange, and green profiles, respectively.

The density fluctuations of neutral gas shown in blue are used to derive turbulence energy dissipation rates, ε, as mentioned in Sec. 2. The resultant ε-profiles for up- and downleg are shown in Figs. 11a and 11b, respectively.

Blue and green profiles represent turbulence derivation utilizing different spectral models, i.e. of Heisenberg (1948) and Tatarskii (1971), respectively (see also e.g., Lübken et al., 1993). The difference between the green and the blue values can

5 be considered as method's uncertainty. The black bold and grey profiles show climatologies, that is mean seasonal values for winter and summer, respectively. Fig. 11 reveals, for instance, that we observed turbulence activity in the entire altitude range from 60 up to 100 km. This is a characteristic feature for winter season. Also the upleg and downleg turbulence data qualitatively agree with each other. Vertical thick lines in Fig. 11 show mean values over the marked altitude regions (i.e., 10 km altitude bins). If compared with results of our previous rocket campaign WADIS-1 that was conducted in summer (Strelnikov

10 et al., 2017), the observed winter turbulence field does not show big difference between up- and downleg measurements. If taking only mean values with their uncertainties in consideration, the height region 70 to 100 km looks very similar on both up- and downleg. The downleg turbulence measurements, however, reveal a patch of very strong turbulence around ∼65 km height.

In Fig. 12 we show wavelet spectrogram of neutral density fluctuations shown in Fig. 10. This spectrum was used to derive

15 the ε-profile shown in Fig. 11b (see Strelnikov et al., 2003, for details). In this spectrogram power falls down along the spatial scale axis from large to small scales. Noise level corresponds to bluish colors. Turbulent layers can be recognized in this figure

(a) Upleg   (b) Downleg
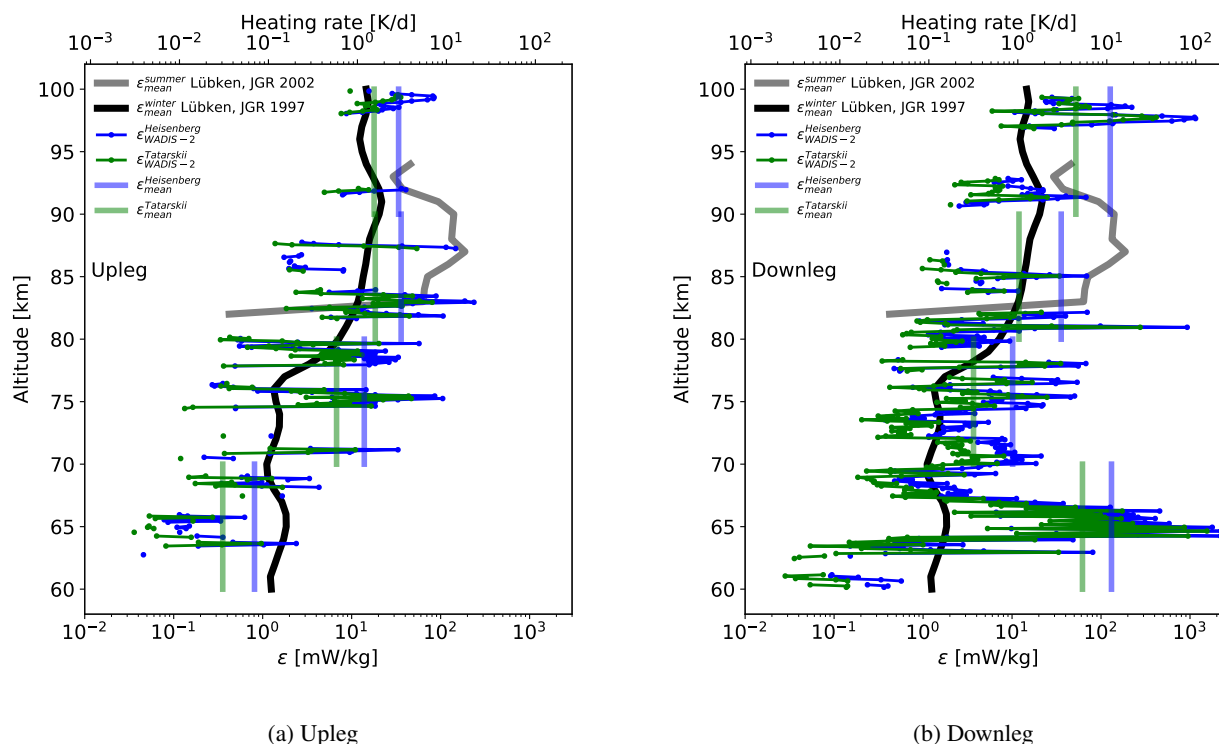
Figure 11. In situ turbulence measurements by the WADIS-2 rocket launched on 1st of March 2015 at 01:44:00 UTC. Blue and green colors represent turbulence energy dissipation rates, ε, derived using spectral models of Heisenberg (1948) and Tatarskii (1971), respectively. Vertical lines show mean ε-values over the 10 km height bins. Bold black and gray profiles show turbulence climatologies for winter and summer, respectively.

as regions of green color which are extended to small-scales of the order of 100 m and less. Note, that this only gives a rough approximate visualization of the turbulence structure. A more close and detailed examination of individual spectra (PSD vs frequency) is required to derive the ε-profile. Nevertheless, colored wavelet spectrograms like those shown in Fig. 12 help to identify power change at different scales in the spectrum. So, one can identify, for instance, two near parallel slopes in red color

5   between ∼80 an ∼98 km that extend approximately from scales of 5 to 3 km down to 1 km and slightly below. This region is marked with the blue dashed oval and tilted dashed lines in Fig. 12. This picture is reminiscent of a GW-saturation process when vertical wavelength of GW becomes shorter. Consistently, we observed a turbulence layer on top of this saturation region, i.e. in 98 to 100 km range.

In Fig. 12 we further compare the neutral density spectrum with the spectrum of atomic oxygen density fluctuations. The

10   black contour on top of the colored scalogram is a constant power line taken from a similarly derived wavelet spectrum (not shown here) of the O-density fluctuations which are shown in Fig. 10. The contour line reproduces the small-scale structure of
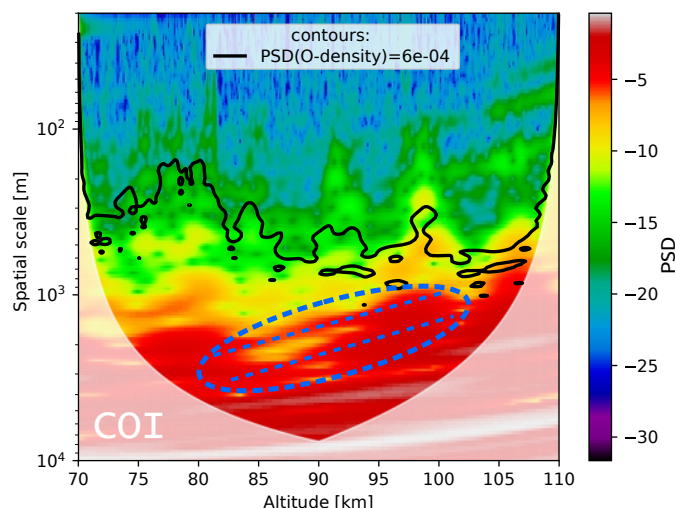
Figure 12. Wavelet spectrum of neutral density fluctuations as color contours. Black contour shows a constant-power line taken from wavelet spectrum of atomic oxygen density fluctuations (not shown here). White shading shows cone of influence (COI). Dashed oval and two lines mark region where power peak shifts from large to small-scales which can be attributed to a GW-saturation process.

neutral density fluctuations quite well. So, all regions where neutral density structures extent to small-scales are also present in the O-density spectra. This suggests that atomic oxygen is affected by turbulent mixing.

In order to directly compare the spectral content of neutral air and atomic oxygen fluctuations we further show in Fig. 13 two dimensional slices of the corresponding wavelet spectrograms (i.e., for neutrals and oxygen). Fig. 13 shows spectra of neutrals and O in black and blue colors, respectively. Additionally, in Fig. 13a we show a Fourier spectrum of the horizontal wind fluctuations (magenta color) shown in Fig. 9. The wind spectrum only extends to ∼200 m which is due to the limited altitude resolution of these measurements. The red dashed line marks slope of k^{-3} (k is wavenumber) which is commonly attributed to gravity waves (Fritts and Alexander, 2003). It is clearly seen that the spectrum of wind fluctuations closely follows the k^{-3} power law. Spectrum of neutrals is also very close to it down to ∼15 m scales where white nose produced by instrument electronics dominates the signal. Dashed green line in Fig. 13a marks $k^{-5/3}$ slope, that is the famous Kolmogorov power law which suggests that turbulence was acting on tracer distribution. It can be seen that the spectrum of O-density fluctuations might have been affected by turbulence.

Fig. 13b shows spectra of neutral and oxygen density fluctuations taken from the region where moderate turbulence was observed near 82 km. Dark blue solid bold line also shows the fitted theoretical model of Heisenberg (1948). This model only describes two parts (or subranges) of turbulence spectrum. Its left part called inertial subrange follows the $k^{-5/3}$ power law whereas the dissipation part often referred to as viscous subrange is described by k^{-7} slope. One can see that the leftmost part of both spectra (i.e., for O and neutrals) follows the k^{-3}, i.e. GW-like slope (also marked by red dashed line) which then smoothly transits into the turbulence spectrum well described by the Heisenberg model. The inertial subrange of both spectra
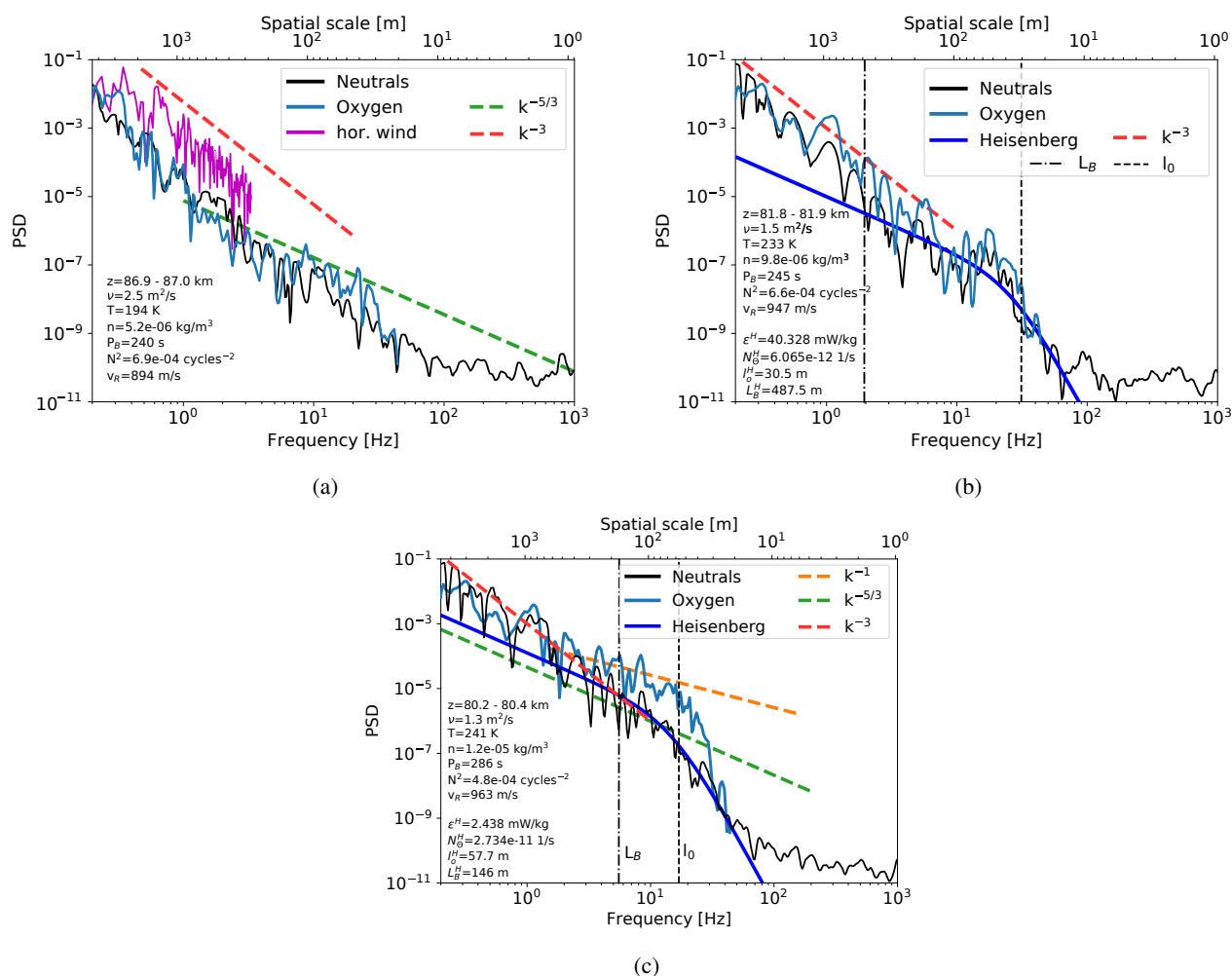
Figure 13. Normalized power spectral densities (PSD) of horizontal wind fluctuations (magenta), $\Delta N_n/N_n$ (black), and $\Delta[O]/[O]$ (blue) measured during descend of WADIS-2 sounding rocket. Dashed red, green, and orange lines show slopes with k^{-3}, $k^{-5/3}$, and k^{-1} power law, respectively. Vertical black dashed and dashed-dotted lines mark inner and buoyancy scales of turbulence, $l_\circ$ and L_B, respectively. a) All spectra reveal k^{-3} slope attributed to gravity waves; b) All spectra reveal both waves and turbulence. The neutral- and O-spectrum are near identical. c) Small-scale part of the O-spectrum reveal a k^{-1} slope.

spans over the same range of spatial scales, namely from $L_B \approx 500$ down to $l_o \approx 30$ m. We recall here, that the ε-value is directly derived from the spatial scale l_o defined as transition between inertial and viscous subranges.

Fig. 13c shows spectra from region just below that one described above. The ε-value here drops by one order of magnitude and the inertial subrange shrinks to ~ 100 m. Interestingly, the atomic oxygen spectrum reveals a somewhat different shape. Fig. 13b and 13c demonstrate two types of spectral behavior of O-density fluctuations inside turbulence layers observed during WADIS-2 rocket experiment.

5 Discussion

In this section we discuss the shown above fluctuations in different quantities measured with rocket-borne and ground-based instruments. First we focus on the large scale morphology in temperature field. Then we discuss fluctuations which might be attributed to gravity waves. Finally, we consider the observed smallest-scale structures due to turbulence.

Fig. 6 shows a prominent temperature enhancement around ~ 100 km altitude. As mentioned in Sec. 3, Szewczyk et al. (2013) observed similar temperature enhancement in the same altitude region. They showed, that this signature was observed by MLS satellite instrument over large region and was also seen in lidar data for long time. These two facts lead them to conclude that the observed temperature enhancement could be qualified as mesospheric inversion layer (MIL). Their lidar temperature measurements also showed that MIL descended together with tide. A striking feature accompanied MIL studied by Szewczyk et al. (2013) was a very strong turbulence layer with $\varepsilon = 2$ W/kg (equivalent to a heating rate of 200 K/day) observed on top of their upper MIL. Interestingly, our downleg data reveal very similar situation. Namely, on top of the temperature enhancement we also observe a vigorous turbulence layer with $\varepsilon \simeq 1$ W/kg (or ~ 100 K/d). This temperature enhancement also descends within a time period of several hours. Its spatial extent is at least 60 km (distance between ascent and descent of the sounding rocket plus the distance to the south-east Na-lidar beam, see Fig. 1). The upleg rocket data, however, are somewhat different. They show similar temperature enhancement, but the turbulence is one order of magnitude weaker. Szewczyk et al. (2013) argued that if turbulence itself did not produce the MIL, it might have amplified it. This statement is consistent with our observations. The weaker turbulence on upleg accompany ~ 10 K colder temperature maximum.

In the previous sections we showed ground-based wind and in-situ density and temperature measurements which reveal signatures of gravity waves. Closer comparison of density fluctuations of neutral gas, positive ions, and atomic oxygen in Fig. 10 shows at least two things. First, the amplitudes of GW in these tracers are different. Second, the phases can be shifted relative to each other. Fritts and Thrane (1990) and Thrane et al. (1994) studied the relationship between ion and neutral density fluctuations due to gravity wave and turbulent motions both theoretically and experimentally. Their results indicated that this relationship in the middle atmosphere ranges between an adiabatic and a chemical equilibrium limit, depending on the characteristics of the wave or turbulent motion and the ion production and recombination rates. In pure adiabatic limit case, that is when fully developed turbulence dominates in observed timeseries, the neutral and ion density fluctuations must be in anti-phase, i.e. shifted by π relative to each other. Fritts and Thrane (1990) also noted that we should not expect the fluctuations

of ions and neutrals to be either in or out of phase. Rather, they will have a phase shift that depends on the relative values of the intrinsic wave frequency, the mean ion number density, and the effective recombination rate.

Fritts and Thrane (1990) showed that the phase shift between fluctuations of different species depends on the relative magnitudes of wave and chemistry time scales. For low frequency waves this phase shift → 0, indicating that the species are in

5 chemical equilibrium. This situation is well observed just above the MIL-like temperature enhancement in the altitude range from 102 to 110 km (see Fig. 10), where all three species, i.e. oxygen, ions, and neutrals show nearly the same oscillations. This behavior is observed directly above the upper turbulence layer measured by rocket-borne instruments on both up- and downleg.

Next, we focus on the feature seen in the wavelet scalogram (Fig. 12) which is marked by the dashed lines. It suggests that

10 waves with vertical wavelength of ∼2–3 km saturated within altitude range ∼80 to 98 km and broke producing turbulence layers (Fig. 11). That is, our new measurements suggest that turbulence produced by breaking GW amplifies temperature fluctuations producing MIL-like signature in temperature field. Note, that density fluctuations in Fig. 10 do not have this large MIL-like signature because of the background subtraction procedure which filtered out waves longer than 5 km.

It is interesting to note, that also the altitude region below ∼82 km reveals feature, similar to what is observed near 100 km

15 height: stronger turbulence activity on downleg accompanies higher temperatures. Furthermore, right above this active region GW-amplitudes seen in temperature data (Fig. 6) are very low. ε-profiles (Fig. 11) also demonstrate lower turbulence activity (which might be connected to low GW-amplitudes). Also wind fluctuations (Fig. 9) are consistent with this picture. Their amplitude grows in the height region 30 to 70 km and afterwards, near 85 km it vanishes.

All these facts together suggest that we observed waves saturation and dissipation in the altitude range 70 to 80 km ac-

20 companied by turbulence production. Above these heights we observed GW-amplitude growth and breakdown near 100 km. The latter can be either attributed to secondary GW generated by turbulence (see e.g., Becker and Vadas, 2018, and references therein) or just another wave package passing through our observation field.

The spatial scales considered in the discussion above are of the order of 1 to few kilometers. This range of vertical scales is characteristic for GW in MLT. If we look at these fluctuations in spectral domain (e.g., shown in Fig 13) we see that they

25 follow the k^{-3} slope (usually attributed to GW) in the range of scales from 5 km down to hundreds of meters. Now we discuss structures at smaller scales. A power increase in spectrum which appears at spatial scales below ∼500 m must rather be attributed to action of turbulence. If the spectrum reveals a clear shape which can be mathematically described by a model (e.g., Heisenberg, 1948; Tatarskii, 1971) we argue that we observed an active turbulence and derive its energy dissipation rate, ε. To do so, we have to make sure, that the density fluctuations that we use for turbulence analysis are passive, that is do not

30 influence the flow and conservative, i.e. its value is not affected by the flow (see e.g., Lübken, 1992, 1997; Lübken et al., 1993, 2002). It was also shown, that plasma density fluctuations can both satisfy this requirement and, under specific conditions, can be affected by non-turbulent processes like enhanced recombination of electrons with cluster ions (e.g., Röttger and La Hoz, 1990), the effect of charged ice particles in PMSE (e.g., Cho et al., 1992), or plasma instabilities (e.g., Blix et al., 1994; Strelnikov et al., 2009). If spectra at small-scales reveal some enhanced power which cannot be described by a model, it might

imply that we observed a residual structuring after action of turbulence some time before. In such a case we cannot derive any parameter of turbulence from this data.

Recalling to above discussion about relationship between density fluctuations of neutrals and ions we note that our analysis results suggest that a similar relationship should also exist between small-scale atomic oxygen density fluctuations and other

5 constituents, i.e. ionospheric plasma and neutral gas. So, e.g., earlier common volume rocket-borne measurements of atomic oxygen and electron densities (N_e) by Friedrich et al. (1999) showed a clear correlation between fine structure of O- and N_e-density profiles.

In the height range from ∼78 to ∼85 km fluctuations of ion density are in phase with those of O-density and they both are almost in anti-phase with the neutrals. This might imply that we here observed O-densities which are in chemical equilibrium

10 with ion densities (phase shift close to zero) located inside turbulence layers (phase shift ∼ π). The turbulence measurements indeed show turbulent layers in this altitude range (see Fig 11b). On the one hand, this supports the theory of Fritts and Thrane (1990), but at the same time it raises the question how O-density behaves inside turbulence and whether turbulence affects the height distribution of atomic oxygen.

Now we discuss the power spectra shown in Fig. 13. This figure demonstrates three types of spectra found in the fluc-

15 tuations measured during the WADIS-2 flight. As noted above, the upper panel shows spectra typical for gravity waves whereas two lower panels demonstrate turbulent spectra. The both spectra in the middle panel, i.e. the PSD($\Delta N_n/N_n$) and the PSD(Δ[O]/[O]) shown with black and blue lines, respectively, are near identical, suggesting that at these altitudes the chemical time constant is larger than the turbulent one. At the same time, just below this height, that is where the chemical time constant is expected to be comparable, the PSD(Δ[O]/[O]) shows different spectral behavior revealing a k^{-1} slope at

20 small-scales.

Friedrich (2016) noted, that O-density should positively correlate with N_e for two reasons: (1) [O] inhibits the formation of water cluster ions (e.g., $H^+(H_2O)_n$) which have significantly faster recombination rates than molecular ions (O_2^+, NO^+) (2) [O] provides a reverse reaction effectively detaching electrons from negative ions. In terms of density fluctuations, N_e is ultimately connected to the ambient ion density, N_i, which, in turn at heights below ∼100 km are essentially governed by collisions

25 with neutrals (e.g., Rapp et al., 2003). That is the small-scale structures produced by turbulence must be observed in these species too. The difference in their response to turbulence arise due to difference of their diffusivity. Thus, diffusion constant of charged constituents is affected by ambipolar forces resulting from electrostatic coupling between positively and negatively charged species (e.g., Chen, 2016). Moreover, it was shown that heavy charged aerosols if present can significantly reduce plasma diffusivity allowing extension of eddy cascade in those species down to much smaller scales (e.g., Rapp et al., 2003).

30 This, for instance can lead to such phenomena like polar mesosphere radar echoes in summer or winter, PMSE or PMWE, respectively (see e.g., Rapp and Lübken, 2004; Lübken et al., 2006). Under conditions when diffusivity, D, of plasma species is considerably reduced its spectral behavior can be described by a model which includes this parameter via e.g., Schmidt number, Sc=ν/D, where ν is kinematic viscosity of ambient gas (e.g., Driscoll and Kennedy, 1985). Such models implement theory of Batchelor (1958) and describe the small-scale part of the spectrum by a k^{-1} power law. In other words, if spectrum

35 of density fluctuations reveals the k^{-1} slope at scales smaller than those where $k^{-5/3}$ is present, this means that the diffusivity

of this constituent is reduced. To summarize, spectra of O-density fluctuations which show the k^{-1} slope (one example of those is shown in Fig. 13c), may imply that atomic oxygen can show different diffusion properties inside turbulence layers. That is, addressing the question whether turbulence affects height distribution of atomic oxygen, we can definitely say yes. The observed k^{-1} spectral behavior, however needs further in depth investigation and lies out of scope of this paper.

6   Conclusions

In this paper we present an overview of the entire scope of measurements conducted in the frame of the WADIS-2 sounding rocket campaign. We also demonstrate the important role of small-scale processes like gravity waves and turbulence in the distribution of O in the MLT region.

We show that all measured quantities, including winds, densities, and temperatures, reveal signatures of both waves and turbulence. Analysis of density fluctuations measured by rocket-borne instruments supported the theory by Fritts and Thrane (1990), but also suggested that a similar relationship might exist between atomic oxygen and other constituents, i.e., plasma and neutrals.

Atomic oxygen inside turbulent layers showed two different spectral behaviors at scales smaller than $\sim$300 m. Some of the O-density spectra reproduce spectra of neutral gas, but some of them show a k^{-1} slope. A more detailed study of such very small scales in O-density data is subject of our future work. In particular, a somewhat higher altitude resolution and enhanced sensitivity of FIPEX sensors may yield more detailed picture for our future rocket experiments.

Author contributions.   M.R., F.J.L. and B.S. designed and directed the project; B.S., M.F., R.L., J.H., M.K., J.G., S.L., S.F., G.B., J.H., A.B., M.J.T. designed and directed the subprojects and related instruments; M.E., M.F., J.H., M.K., G.B., B.P.W., H.A., R.L., J.H., R.W., A.B., M.J.T, P.D.P performed the experiments; B.S., M.E., M.F., J.H., G.B., B.P.W., T.S., H.A., I.S., R.L., M.G., J.H., R.W., A.B., M.J.T, P.D.P analyzed the data; All authors contributed to the final manuscript.

Competing interests.   The authors declare that they have no conflict of interest.

Acknowledgements.   This work was supported by the German Space Agency (DLR) under grant 50 OE 1001 (Project WADIS). Authors thank DLR-MORABA for their excellent contribution to the project by developing the complicated WADIS payloads and campaigns support together with the Andøya Space Center. Authors thank H.-J. Heckl and T. Köpnick for building the IAP rocket instrumentation. The design and initial development of the AMTM was supported under an AFOSR DURIP grant to USU. The AMTM installation and operations at ALOMAR were supported under the NSF collaborative grant AGS-1042227.

References

Alexander, M. J., Geller, M., McLandress, C., Polavarapu, S., Preusse, P., Sassi, F., Sato, K., Eckermann, S., Ern, M., Hertzog, A., Kawatani, Y., Pulido, M., Shaw, T. A., Sigmond, M., Vincent, R., and Watanabe, S.: Recent developments in gravity-wave effects in climate models and the global distribution of gravity-wave momentum flux from observations and models, Quarterly Journal of the Royal Meteorological

5   Society, 136, 1103–1124, https://doi.org/10.1002/qj.637, https://rmets.onlinelibrary.wiley.com/doi/abs/10.1002/qj.637, 2010.

Asmus, H., Staszak, T., Strelnikov, B., Lübken, F.-J., Friedrich, M., and Rapp, M.: Estimate of size distribution of charged MSPs measured in situ in winter during the WADIS-2 sounding rocket campaign, Annales Geophysicae, 35, 979–998, https://doi.org/10.5194/angeo-35-979-2017, 2017.

Batchelor, G. K.: Small scale variation of convected quantities like temperature in turbulent field, J. Fluid Mech., 5, 113–133, 1958.

10   Becker, E. and Schmitz, G.: Energy Deposition and Turbulent Dissipation Owing to Gravity Waves in the Mesosphere., Journal of Atmospheric Sciences, 59, 54–68, https://doi.org/10.1175/1520-0469(2002)059<0054:EDATDO>2.0.CO;2, 2002.

Becker, E. and Vadas, S. L.: Secondary gravity waves in the winter mesosphere: Results from a high-resolution global circulation model, J. Geophys. Res., 123, 2605–2627, https://doi.org/10.1002/2017JD027460, 2018.

Blix, T. A., Thrane, E. V., Kirkwood, S., and Schlegel, K.: Plasma instabilities in the lower E-region observed during the DYANA campaign,

15   J. Atmos. Terr. Phys., 56, 1853–1870, 1994.

Caridade, P. J. S. B., Horta, J.-Z. J., and Varandas, A. J. C.: Implications of the O + OH reaction in hydroxyl nightglow modeling, Atmospheric Chemistry & Physics, 13, 1–13, https://doi.org/10.5194/acp-13-1-2013, 2013.

Chen, F. F.: Introduction to Plasma Physics and Controlled Fusion, https://doi.org/10.1007/978-3-319-22309-4, 2016.

Cho, J. Y. N., Hall, T. M., and Kelley, M. C.: On the role of charged aerosols in polar mesosphere summer echoes, J. Geophys. Res., 97,

20   875–886, 1992.

Driscoll, R. J. and Kennedy, L. A.: A model for the spectrum of passive scalars in an isotropic turbulence field, Phys. Fluids, 28, 72–80, 1985.

Eberhart, M., Löhle, S., Steinbeck, A., Binder, T., and Fasoulas, S.: Measurement of atomic oxygen in the middle atmosphere using solid electrolyte sensors and catalytic probes, Atmospheric Measurement Techniques, 8, 3701–3714, https://doi.org/10.5194/amt-8-3701-2015,

25   2015.

Eberhart, M., Löhle, S., Strelnikov, B., , Fasoulas, S., Lübken, F.-J., Rapp, M., Hedin, J., Khaplanov, M., and Gumbel, J.: Atomic oxygen number densities in the MLT region measured by solid electrolyte sensors on WADIS-2, Atmospheric Measurement Techniques, submitted, this issue, 2018.

Egito, F., Takahashi, H., and Miyoshi, Y.: Effects of the planetary waves on the MLT airglow, Annales Geophysicae, 35, 1023–1032,

30   https://doi.org/10.5194/angeo-35-1023-2017, https://www.ann-geophys.net/35/1023/2017/, 2017.

Friedrich, M.: Handbook of the Lower Ionosphere, Verlag der Technischen Universität Graz, https://doi.org/10.3217/ 978-3-85125-485-3, https://lampx.tugraz.at/~karl/verlagspdf/ionosphere_friedrich_ebook.pdf, 2016.

Friedrich, M., Gumbel, J., and Pilgram, R.: Atomic Oxygen in the Mesosphere and its Relevance for the Ionosphere: A Summary of Empirical Evidence, in: European Rocket and Balloon Programs and Related Research, edited by Kaldeich-Schürmann, B., vol. 437 of *ESA Special*

35   *Publication*, p. 287, 1999.

Fritts, D. C. and Alexander, M. J.: Gravity wave dynamics and effects in the middle atmosphere, Reviews of Geophysics, 41, 1003, https://doi.org/10.1029/2001RG000106, 2003.

Fritts, D. C. and Thrane, E. V.: Computation of the ion/neutral density ratio in the presence of wave and chemical effects, Journal of Atmospheric and Terrestrial Physics, 52, 827–834, https://doi.org/10.1016/0021-9169(90)90019-J, 1990.

Fritts, D. C., Pautet, P.-D., Bossert, K., Taylor, M. J., Williams, B. P., Iimura, H., Yuan, T., Mitchell, N. J., and Stober, G.: Quantifying gravity wave momentum fluxes with Mesosphere Temperature Mappers and correlative instrumentation, Journal of Geophysical Research (Atmospheres), 119, 13, https://doi.org/10.1002/2014JD022150, 2014.

Hedin, J., Gumbel, J., Stegman, J., and Witt, G.: Use of O_2 airglow for calibrating direct atomic oxygen measurements from sounding rockets, Atmospheric Measurement Techniques, 2, 801–812, 2009.

Heisenberg, W.: Zur statistischen Theorie der Turbulenz, Z. Physik, 124, 628–657, 1948.

Hines, C. O. and Tarasick, D. W.: On the detection and utilization of gravity waves in airglow studies, Planetary and Space Science, 35, 851–866, https://doi.org/10.1016/0032-0633(87)90063-8, 1987.

Latteck, R. and Strelnikova, I.: Extended observations of polar mesosphere winter echoes over Andøya (69∘N) using MAARSY, Journal of Geophysical Research (Atmospheres), 120, 8216–8226, https://doi.org/10.1002/2015JD023291, 2015.

Latteck, R., Singer, W., Rapp, M., Vandepeer, B., Renkwitz, T., Zecha, M., and Stober, G.: MAARSY: The new MST radar on Andøya-System description and first results, Radio Science, 47, RS1006, https://doi.org/10.1029/2011RS004775, 2012.

Lednyts'kyy, O., von Savigny, C., Eichmann, K.-U., and Mlynczak, M. G.: Atomic oxygen retrievals in the MLT region from SCIAMACHY nightglow limb measurements, Atmospheric Measurement Techniques, 8, 1021–1041, https://doi.org/10.5194/amt-8-1021-2015, 2015.

Lübken, F.-J.: On the extraction of turbulent parameters from atmospheric density fluctuations, J. Geophys. Res., 97, 20,385–20,395, 1992.

Lübken, F.-J.: Seasonal variation of turbulent energy dissipation rates at high latitudes as determined by insitu measurements of neutral density fluctuations, J. Geophys. Res., 102, 13,441–13,456, 1997.

Lübken, F.-J., Hillert, W., Lehmacher, G., and von Zahn, U.: Experiments revealing small impact of turbulence on the energy budget of the mesosphere and lower thermosphere, J. Geophys. Res., 98, 20,369–20,384, 1993.

Lübken, F.-J., Rapp, M., and Hoffmann, P.: Neutral air turbulence and temperatures in the vicinity of polar mesosphere summer echoes, J. Geophys. Res., 107(D15), 4273–4277, https://doi.org/10.1029/2001JD000 915, 2002.

Lübken, F.-J., Strelnikov, B., Rapp, M., Singer, W., Latteck, R., Brattli, A., Hoppe, U.-P., and Friedrich, M.: The thermal and dynamical state of the atmosphere during polar mesosphere winter echoes, Atmos. Chem. Phys., 6, 13–24, 2006.

Marsh, D. R., Smith, A. K., Mlynczak, M. G., and Russell, J. M.: SABER observations of the OH Meinel airglow variability near the mesopause, Journal of Geophysical Research (Space Physics), 111, A10S05, https://doi.org/10.1029/2005JA011451, 2006.

McDade, I. C.: The photochemistry of the MLT oxygen airglow emissions and the expected influences of tidal perturbations, Advances in Space Research, 21, 787–794, https://doi.org/10.1016/S0273-1177(97)00674-1, 1998.

McDade, I. C., Murtagh, D. P., Greer, R. G. H., Dickinson, P. H. G., Witt, G., Stegman, J., Llewellyn, E. J., Thomas, L., and Jenkins, D. B.: ETON 2 - Quenching parameters for the proposed precursors of O2(b1Sigma + g) and O(1S) in the terrestrial nightglow, Planetary and Space Science, 34, 789–800, https://doi.org/10.1016/0032-0633(86)90075-9, 1986.

McKinnell, L.-A. and Friedrich, M.: A neural network-based ionospheric model for the auroral zone, Journal of Atmospheric and Solar-Terrestrial Physics, 69, 1459–1470, https://doi.org/10.1016/j.jastp.2007.05.003, 2007.

Mlynczak, M. G. and Solomon, S.: Middle atmosphere heating by exothermic chemical reactions involving odd-hydrogen species, Geophysical Research Letters, 18, 37–40, https://doi.org/10.1029/90GL02672, https://agupubs.onlinelibrary.wiley.com/doi/abs/10.1029/90GL02672, 1991.

Mlynczak, M. G. and Solomon, S.: A detailed evaluation of the heating efficiency in the middle atmosphere, J. Geophys. Res., 98, 10, https://doi.org/10.1029/93JD00315, 1993.

Pautet, P.-D., Taylor, M. J., Pendleton, W. R., Zhao, Y., Yuan, T., Esplin, R., and McLain, D.: Advanced mesospheric temperature mapper for high-latitude airglow studies, Appl. Optics, 53, 5934, https://doi.org/10.1364/AO.53.005934, 2014.

5   Picone, J. M., Hedin, A. E., Drob, D. P., and Aikin, A. C.: NRLMSISE-00 empirical model of the atmosphere: Statistical comparisons and scientific issues, Journal of Geophysical Research (Space Physics), 107, 1468, https://doi.org/10.1029/2002JA009430, 2002.

Rapp, M. and Lübken, F.-J.: Polar mesosphere summer echoes (PMSE): Review of observations and current understanding, Atmos. Chem. Phys., 4, 2601–2633, 2004.

Rapp, M., Lübken, F.-J., and Blix, T. A.: Small scale density variations of electrons and charged particles in the vicinity of po-

10   lar mesosphere summer echoes, Atmospheric Chemistry and Physics, 3, 1399–1407, https://doi.org/10.5194/acp-3-1399-2003, https://www.atmos-chem-phys.net/3/1399/2003/, 2003.

Rapp, M., Strelnikov, B., Müllemann, A., Lübken, F.-J., and Fritts, D. C.: Turbulence measurements and implications for gravity wave dissipation during the MaCWAVE/MIDAS rocket program, Geophys. Res. Lett., 31, L24S07, https://doi.org/10.1029/2003GL019325, 2004.

15   Rapp, M., Latteck, R., Stober, G., Hoffmann, P., Singer, W., and Zecha, M.: First three-dimensional observations of polar mesosphere winter echoes: Resolving space-time ambiguity, J. Geophys. Res., 116, A11307, https://doi.org/10.1029/2011JA016858, 2011.

Röttger, J. and La Hoz, C.: Characteristics of polar mesosphere summer echoes (PMSE) observed with the EISCAT 224 MHz radar and possible explanations of their origin, Journal of Atmospheric and Terrestrial Physics, 52, 893–906, 1990.

Smith, A. K., Marsh, D. R., Mlynczak, M. G., and Mast, J. C.: Temporal variations of atomic oxygen in the upper mesosphere from SABER,

20   Journal of Geophysical Research (Atmospheres), 115, D18309, https://doi.org/10.1029/2009JD013434, 2010.

Snively, J. B.: Mesospheric hydroxyl airglow signatures of acoustic and gravity waves generated by transient tropospheric forcing, Geophysical Research Letters, 40, 4533–4537, https://doi.org/10.1002/grl.50886, 2013.

Strelnikov, B., Rapp, M., and Lübken, F.-J.: A new technique for the analysis of neutral air density fluctuations measured in situ in the middle atmosphere, Geophysical Research Letters, 30, 2052, https://doi.org/doi:10.1029/2003GL018271, 2003.

25   Strelnikov, B., Rapp, M., Zecha, M., Blix, T. A., Friedrich, M., and Yeoman, T. K.: PMSE and E-region plasma instability: In situ observations, Journal of Atmospheric and Solar-Terrestrial Physics, 71, 143–157, https://doi.org/10.1016/j.jastp.2008.10.003, 2009.

Strelnikov, B., Rapp, M., and Lübken, F.: In-situ density measurements in the mesosphere/lower thermosphere region with the TOTAL and CONE instruments, pp. 1–11, Terrapub, https://doi.org/10.5047/aisi.001, 2013.

Strelnikov, B., Szewczyk, A., Strelnikova, I., Latteck, R., Baumgarten, G., Lübken, F.-J., Rapp, M., Fasoulas, S., Löhle, S., Eberhart, M.,

30   Hoppe, U.-P., Dunker, T., Friedrich, M., Hedin, J., Khaplanov, M., Gumbel, J., and Barjatya, A.: Spatial and temporal variability in MLT turbulence inferred from in situ and ground-based observations during the WADIS-1 sounding rocket campaign, Annales Geophysicae, 35, 547–565, https://doi.org/10.5194/angeo-35-547-2017, 2017.

Strelnikova, I., Baumgarten, G., and Lüebken, F.-J.: Advanced hodograph-based analysis technique to derive gravity waves parameters, Atmos. Meas. Tech., https://doi.org/submitted, 2018.

35   Szewczyk, A., Strelnikov, B., Rapp, M., Strelnikova, I., Baumgarten, G., Kaifler, N., Dunker, T., and Hoppe, U.-P.: Simultaneous observations of a Mesospheric Inversion Layer and turbulence during the ECOMA-2010 rocket campaign, Ann. Geophys., 31, 775–785, https://doi.org/10.5194/angeo-31-775-2013, 2013.

Tatarskii, V. I.: The effects of the turbulent atmosphere on wave propagation, Jerusalem: Israel Program for Scientific Translations, 1971.

Taylor, M. J., Bishop, M. B., and Taylor, V.: All-sky measurements of short period waves imaged in the OI(557.7 nm), Na(589.2 nm) and near infrared OH and O_2(0,1) nightglow emissions during the ALOHA-93 Campaign, Geophysical Research Letters, 22, 2833–2836, https://doi.org/10.1029/95GL02946, 1995.

Taylor, M. J., Pendleton, W. R., Clark, S., Takahashi, H., Gobbi, D., and Goldberg, R. A.: Image measurements of short-period gravity waves at equatorial latitudes, Journal of Geophysical Research, 102, 26, https://doi.org/10.1029/96JD03515, 1997.

Taylor, M. J., Pautet, P.-D., Medeiros, A. F., Buriti, R., Fechine, J., Fritts, D. C., Vadas, S. L., Takahashi, H., and São Sabbas, F. T.: Characteristics of mesospheric gravity waves near the magnetic equator, Brazil, during the SpreadFEx campaign, Annales Geophysicae, 27, 461–472, https://doi.org/10.5194/angeo-27-461-2009, 2009.

Thrane, E. V., Blix, T. A., Hoppe, U.-P., Lübken, F.-J., Hillert, W., Lehmacher, G., and Fritts, D. C.: A study of small-scale waves and turbulence in the mesosphere using simultaneous in situ observations of neutral gas and plasma fluctuations, Journal of Atmospheric and Terrestrial Physics, 56, 1797–1808, https://doi.org/10.1016/0021-9169(94)90011-6, 1994.

Torr, D. G.: The photochemistry of the upper atmosphere, pp. 165–278, 1985.

von Zahn, U., Thrane, E. V., and Skatteboe, R.: The ALOMAR facility: Status and outlook, in: Proceedings of the 12th ESA Symposium on European Rocket and Balloon Programmes and Related Research, edited by Blix, T. A., vol. ESA SP–370, pp. 379–385, Lillehammer, Norway, 1995.

Walterscheid, R. L., Schubert, G., and Straus, J. M.: A dynamical-chemical model of wave-driven fluctuations in the OH nightglow, Journal of Geophysical Research, 92, 1241–1254, https://doi.org/10.1029/JA092iA02p01241, 1987.

Wörl, R., Strelnikov, B., Viehl, T., Höffner, J., Pautet, P.-D., Taylor, M., and Lübken, F.: Thermal structure of the mesopause region during the WADIS-2 rocket campaign, Atmospheric Chemistry and Physics, submitted, 2018.